Study of magnetic fields and current in the Z pinch at stagnation

Cite as: Phys. Plasmas **22**, 092710 (2015); https://doi.org/10.1063/1.4931079
Submitted: 04 July 2015 . Accepted: 03 September 2015 . Published Online: 22 September 2015

V. V. Ivanov, A. A. Anderson, D. Papp, A. L. Astanovitskiy, V. Nalajala, and O. Dmitriev

Study of magnetic fields and current in the Z pinch at stagnation

V. V. Ivanov,[1] A. A. Anderson,[1] D. Papp,[1,2] A. L. Astanovitskiy,[1] V. Nalajala,[1] and O. Dmitriev[1]
[1]*Department of Physics, University of Nevada, Reno, Nevada 89557, USA*
[2]*ELI-ALPS, ELI-Hu Nkft., H-6720 Szeged, Hungary*
[3]*Blackett Laboratory, Imperial College, London SW7 2BZ, United Kingdom*

(Received 4 July 2015; accepted 3 September 2015; published online 22 September 2015)

The structure of magnetic fields in wire-array Z pinches at stagnation was studied using a Faraday rotation diagnostic at the wavelength of 266 nm. The electron plasma density and the Faraday rotation angle in plasma were calculated from images of the three-channel polarimeter. The magnetic field was reconstructed with Abel transform, and the current was estimated using a simple model. Several shots with wire-array Z pinches at 0.5–1.5 MA were analyzed. The strength of the magnetic field measured in plasma of the stagnated pinch was in the range of 1–2 MG. The magnetic field and current profile in plasma near the neck on the pinch were reconstructed, and the size of the current-carrying plasma was estimated. It was found that current flowed in the large-size trailing plasma near the dense neck. Measurements of the magnetic field near the bulge on the pinch also showed current in trailing plasma. A distribution of current in the large-size trailing plasma can prevent the formation of multi-MG fields in the Z pinch. © *2015 AIP Publishing LLC*.
[http://dx.doi.org/10.1063/1.4931079]

I. INTRODUCTION

Wide investigation of Z pinches arose as a part of controlled fusion research. Later, the interest in dense Z pinches was supported by research in high-energy-density physics, atomic and radiation physics, and laboratory astrophysics. Wire-array Z pinches can generate record power and energy of soft and keV x-ray radiation with high wall-plug efficiency.[1–4] Radiative properties and parameters of plasma strongly depend on the distribution and dynamics of current in the Z pinch. Employment of strong magnetic fields can improve plasma conditions for fusion. Compression and heating of the magnetized plasma is a basis for the pulsed power approach to the controlled fusion.[5]

Magnetic fields in Z pinches have been measured by magnetic probes or by the Faraday rotation in a fiber placed inside the wire array at the early stage.[6–8] Optical Zeeman-split emission lines were used for the measurement of the evolution of the azimuthal magnetic field in the gas-puff plasma.[9] A distribution of the magnetic field was measured down to the 5 mm radius of the oxygen Z pinch on a 0.5 MA generator. Recently, proton deflectometry was applied to plasma in the wire array.[10] A radial Z pinch was probed by the laser-produced proton beam with energy of 4.4 MeV.

A Faraday rotation of the polarization plane of the laser beam in plasma has been used for measurement of the magnetic field in laser-produced and Z-pinch plasmas. Faraday rotation diagnostics in the optical range were applied to plasma in the precursor, single-wire, and fiber Z pinch at current of 100–150 kA elsewhere.[11–13] Bubble-like magnetically active structures were found in the precursor and pinch plasmas in Refs. 11 and 14. An effect of "disappearance" of current in the neck on the fiber Z-pinch was reported in Ref. 12. The authors suggested that main current switched to the external plasma, which was not seen with interferometry at the wavelength of 532 nm. From another side, authors of the later publication reported that 70% of total current flows in the fiber Z pinch.[13] The Faraday rotation diagnostic at 532 nm was also used with a wavefront analyzer for imploding plasma density and current profile measurements in a gas-puff Z pinch.[15]

Wire-array Z pinches at current $\geq$1 MA were less investigated due to high plasma density in the pinch. Strong absorption and refraction in the dense Z pinch plasma are the main issues of laser diagnostics at the wavelength 532 nm. Typically, the laser beam does not penetrate into the stagnated Z pinch and shows only a contour of the trailing plasma around the pinch. The Faraday rotation diagnostic at the wavelength of 266 nm was applied to the stagnated Z pinch at the Zebra pulsed power generator in the University of Nevada, Reno. Ultraviolet (UV) laser diagnostics shows a strong advantage compared to optical probing and can deliver new data about the 1 MA Z pinch at all stages.[16,17] A structure of MG magnetic fields and current distribution in wire-array Z pinches can be reconstructed with UV Faraday diagnostics.[18] The magnetic field and current profile were studied in Z pinches produced by cylindrical wire arrays in the area with strong kink, $m = 1$ MHD instability. It was found that a part of current switch from the main pinch to the additional channel in the trailing plasma presumably due to the increased inductance of the kink.

In this paper, profiles of the magnetic field and current were studied in necks and bulges produced by sausage, $m = 0$ MHD instability in wire-array Z pinches at currents up to 1.5 MA. Z pinches with strong sausage instability were produced by implosions of star and compact cylindrical wire arrays. Magnetic fields $B = 1$–2 MG were reconstructed with a Faraday rotation diagnostic at the wavelength of 266 nm. A distribution of current in Z-pinch plasma was estimated

using simple models of current in the plasma column. It was found that current flowed in the trailing plasma with the lower density. In the vicinity of the neck, current also flowed in the trailing plasma but the current density was higher in the dense neck. In areas with bulges, current flowed in plasma with a larger size compared to the dense pinch. Strong magnetic fields with $B \gg 1$ MG were not found in Z pinches presumably due to distribution of current in the wide area of trailing plasma.

II. EXPERIMENTAL SETUP AND PLASMA DIAGNOSTICS

The experiments were performed at the Zebra pulsed power generator at the Nevada Terawatt Facility (NTF). The Zebra generator produced a current pulse with an 80 ns rising edge (10%–90%) and maximum current of 1 MA on the impedance of 1.9 Ω. One series of experiments was performed at 1.4–1.6 MA current with a load current multiplier (LCM).[19,20]

X-ray diagnostics at the Zebra vacuum chamber included a time-gated pinhole camera, time-integrating spectrometer, Ni bolometer, filtered x-ray diodes (XRDs), and photo-conducting detectors (PCDs).[17] A keV x-ray pulse from PCD filtered by Be 8 μm foil was used in timing diagrams to identify the pinch stage. A six-frame pinhole camera provided two sets of images at two energy ranges of $E_1 > 0.8$ keV and $E_2 > 3$ keV, and the duration of the frames was 2–3 ns. The time integrating spatially resolved spectrometer with a convex potassium hydrogen phthalate (KAP) crystal was used for measurement of plasma electron temperature and density.

Laser diagnostics of the Z pinch included one probing direction for UV diagnostics at 266 nm and another direction for 2-frame shadowgraphy at 532 nm with the angle of 22.5° between directions. UV diagnostics operated as a Faraday rotation diagnostics in these shots. A three-channel polarimeter with shadowgraphy, the Faraday channel, and differential air-wedge interferometer[21] with three UV charge-coupled device (CCD) cameras was described elsewhere.[22–24] An UV polarizer was inserted in the laser path before the vacuum chamber to create a beam with a high-contrast linear polarization. A crystal wedge was installed at the output window for angular separation of the shadow and Faraday rotation channels. Channels in the polarimeter were split by both the angular separation of beams and additional polarizers on CCDs to provide a high contrast in the Faraday channel with small intensity of the laser beam. A field of view of UV diagnostic was $8 \times 8\,\text{mm}^2$ with spatial resolution of 15 μm. A central area of the stagnated Z pinches was investigated. A diagnostic laser produced probing pulses with durations of 0.2 ns at wavelengths of 532 and 266 nm and individual delay lines. Laser channels at 532 and 266 nm were spatially co-aligned using a removable needle placed in the center of the wire array before the shot. Reference images were recorded in all laser channels before the main shot with the Zebra generator.

Aluminum (alloy 5056) star wire-array loads and cylindrical compact wire arrays were investigated. Star wire arrays implode in the cascade manner and produce more homogeneous pinch with smaller trailing plasma at the Zebra generator.[25] Implosions in compact wire arrays at the Zebra generator produce a pinch with numerous necks,[26] which were studied with Faraday rotation diagnostics in this paper.

III. EXPERIMENTAL STUDY OF MAGNETIC FIELDS IN THE Z PINCH

Measurement of the magnetic field and reconstruction of the current distribution near the Z pinch neck are described in Section III A. Measurement of the magnetic field and total current on the bulge of star wire-array Z pinch is presented in Section III B. The magnetic field and current profile in the Z pinch at current 1.4–1.6 MA are studied in Section III C.

A. The magnetic field and current distribution in the vicinity of the neck on the pinch

Distribution of current in bulges and necks of the Z pinch determines general dynamics of plasma and radiation of the pinch at stagnation. The stagnation phase is not static and can include secondary implosions and collapse of hot spots.[18,24] Necks and micropinches with a diameter 60–300 μm are well seen in wire-array Z pinches with UV laser diagnostics.[16,24] A simple estimation shows that necks could generate the magnetic field $B > 10$ MG if, for example, 0.5 MA current flows in the neck 0.2 mm in diameter. From another side, authors of paper[12] claim a "disappearance" of current in the neck on the fiber Z pinch at 0.1 MA current. Laser diagnostics at the wavelength of 266 nm allows measurement of magnetic fields in the 1 MA pinch due to significantly smaller absorption, refraction, phase shift, and Faraday rotation angle in plasma compared to diagnostics at 532 nm.[22]

Necks in compact wire arrays are investigated for magnetic fields. Figure 1 shows a shadowgram of the pinch (a) and magnified fragments with a neck taken in three channels of the polarimeter. Dashed curves are contouring a selected neck in images (b)–(d). The Z pinch is produced by the implosion of the Al cylindrical load, 3 mm in diameter with a mass of 56 μg. Small-diameter loads implode at the rising edge of the current pulse as it is seen in the timing diagram (e). Dotted horizontal lines in images (b) and (c) show the direction of the measurement of the Faraday rotation angle and phase shift in plasma near the neck. Lightening and darkening due to the Faraday rotation effect are seen in the right and left sides of the pinch, respectively. Lightening and darkening in the Faraday image identify magnetic fields with opposite directions.

Figure 2 presents the Faraday rotation angle β, plasma electron density N_e, and magnetic field B calculated along the dotted line in Figs. 1(b)–1(d). The rotation angle is calculated using the shadowgram, Faraday image, and reference images taken before the Z-pinch shot.[22] Intensity of plasma self-emission and a CCD bias are subtracted from intensity of the laser beam. A contrast of the polarimeter is measured $\sim 10^{-4}$. In experiments at the 1 MA regime of the Zebra generator, typical angles of the Faraday rotation in Z-pinch plasma are in the range of 4°–7°. The plasma electron

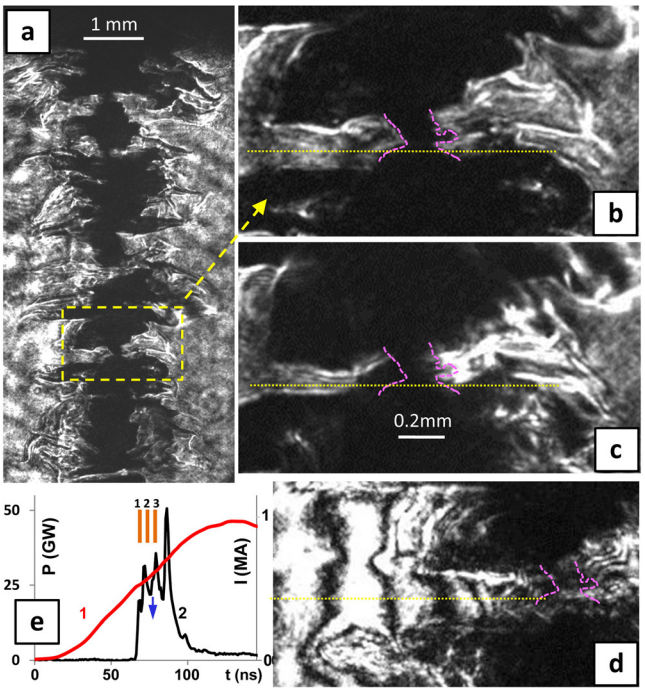

FIG. 1. Laser images of the (a) Z pinch and (b)-(d) a vicinity of the neck in shot 2704. Images (b), (c), and (d) present the shadowgram, Faraday rotation image, and interferogram, respectively. (e) A timing diagram with the current pulse (1), x-ray pulse (2), laser pulse (arrow), and x-ray frames (strips 1–3). A mismatch angle of polarizers is 7.6°.

density, N_e, is reconstructed from the differential interferogram in Fig. 1(d). Three filled areas in Figure 2(a) present the area with opaque plasma (3), area with high plasma density and gradients (2), and area with a small rotation angle and plasma density (1). Light in the opaque zone (3) is a result of stray rays in Z-pinch plasma. This area cannot be used for calculations of the rotation angle and plasma density. Zone (2) is also excluded due to high gradients and complicated tangled structure of interferometric fringes, which disappear near the opaque zone (3). The issue of zone (1) is a high error in the calculated B-field. The rotation angle may be smaller than the noise in this area. The rotation angle in area (1) is approximated by the fitting line to provide smooth approaching of $\beta(r)$ to zero at the edge of the plasma column with $N_e(R_0) = 0$.

Experimental lines $\beta(r)$ and $N_e(r)$ are substituted to the appropriate fitting lines in further calculation. Using smooth fitting lines is necessary due to the high sensitivity of the reconstruction procedure to small peaks on initial functions $\beta(r)$ and $N_e(r)$. By this way, features in initial lines are excluded and only the smoothed field $B(r)$ is calculated. The magnetic field in plasma is reconstructed using the Abel inversion formula

$$\frac{B(r)N_e(r)}{r} = -\frac{2}{\pi\kappa}\int_y^{R_0}\frac{d}{dy}\left(\frac{\beta(y)}{y}\right)\frac{dy}{\sqrt{y^2-r^2}}, \qquad (1)$$

where R_o is the radius of the plasma column and the coefficient $\kappa = 2e^3\lambda^2/(\pi m^2c^4)$, in Gaussian units. The reconstructed magnetic field with a maximum field strength of 1.1 MG is displayed in Fig. 2(d).

The reconstructed magnetic field is compared with the magnetic field of current flowing in a homogeneous plasma column. Lines (1) and (2) in Figure 3(a) show profiles of magnetic fields produced by 0.5 MA (1) and 0.2 MA current flowing in the 0.2 mm neck. A comparison of lines (1) and (2) with the reconstructed field $B(r)$, line (3) shows a strong disagreement. This means that current flows in the wider area of Z-pinch plasma.

The dashed line in Figure 3(b) presents the magnetic field of current with the constant current density profile. This line fits the experimental line if current $I = 0.33$ MA and the diameter of plasma is 1.32 mm. The dotted line presents the magnetic field of the same total current but the current

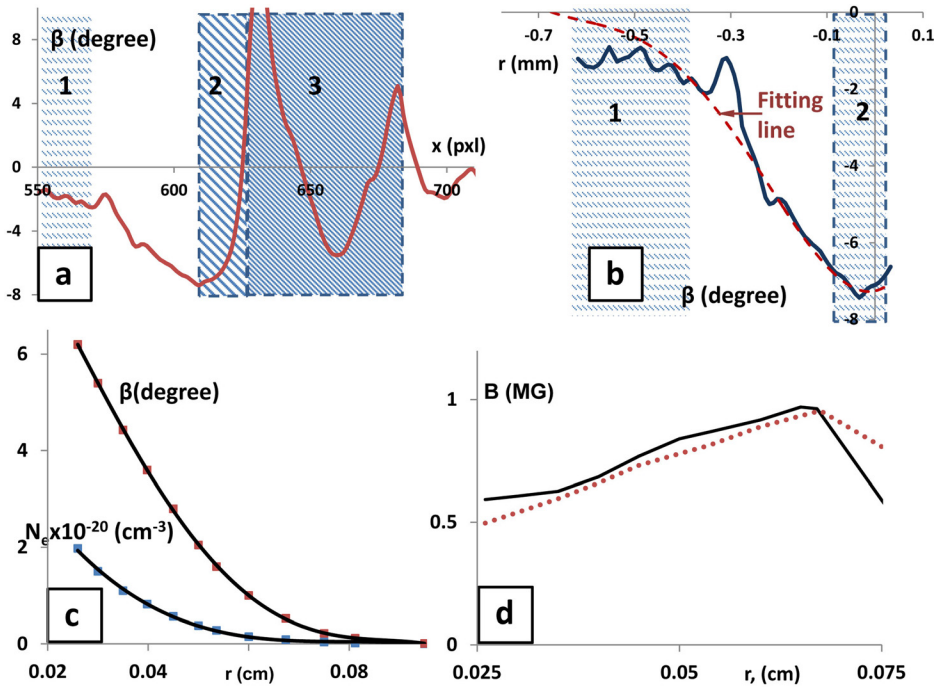

FIG. 2. (a) and (b) Faraday rotation angle in Z-pinch plasma calculated along the dash line in Figs. 1(b) and 1(c). (c) Fitting lines for the Faraday rotation angle and plasma electron density. (d) The reconstructed magnetic field, solid line, and B-field estimated by formula (2), dotted line.

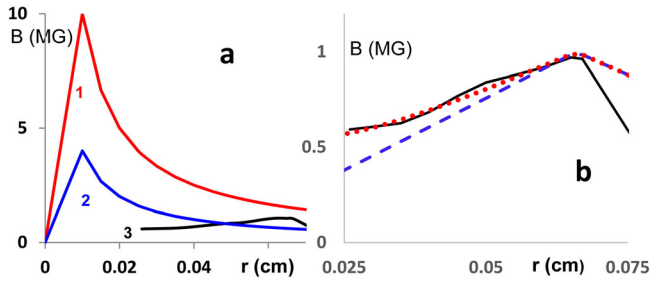

FIG. 3. (a) Comparison of the modelled magnetic field produced by currents of 0.5 MA (1) and 0.2 MA (2) flowing in the plasma neck 0.2 mm in diameter and reconstructed magnetic field (3). (b) Comparison of the reconstructed magnetic field (solid line) with the B-field calculated for constant current density (dashed line) and with the enhanced current density in the neck (dotted line).

density is enhanced in the 0.2 mm neck with a factor of 5. This distribution of current better fits the experimental curve. In this case, the main portion of current flows in a large-size trailing plasma. The enhanced current in the neck is in agreement with bright radiation of necks seen in x-ray images, Figure 4. Position of necks in the UV shadowgram correlates with keV x-ray bright spots. The accuracy of measurements is estimated to be $\pm 25\%$. It includes the impact of the noise in the Faraday image and the error of deviation of the plasma profile from the cylindrical symmetry. The calculated current in the plasma column with radius $R_0 = 1.32$ mm gives only 66% of the total current, measured at this moment by B-dots. The discrepancy can be explained by current in the low-density plasma located at the radius $> R_0$. Low-density plasma is not seen by UV diagnostics but is seen in shadowgram (a) at the wavelength of 266 nm.

The magnetic field can also be estimated from experimental data using the approximate formula for the average magnetic field[14,27]

$$B_a(r) = \frac{1.7\beta(r)}{\lambda\delta(r)}, \tag{2}$$

where $B_a(r)$ is a magnetic field in kG, $\beta(r)$ is a rotation angle in radians, λ is a laser wavelength in cm, and $\delta(r)$ is a phase shift in lines. The magnetic field calculated by formula (2) deviates 5%–10% down from the reconstructed B-field near the maximum [dotted line in Fig. 2(b)]. This estimation is also sensitive to peaks on $\delta(r)$ and $\beta(r)$ curves and should be applied to smooth curves.

We note that necks in the wire-array Z pinch are produced by both the implosion inhomogeneity and sausage instability. Comparison of laser and x-ray images of the pinch shows the formation of necks in points where the implosion plasma bubbles collide at the axis of the wire array.[26,28] In compact wire arrays, the initial configuration of the Z pinch, trailing plasma, and profile of current is impacted by the secondary implosion and plasma motion in the stagnated pinch.[18] Necks can exist during >10 ns and are seen in the x-ray images due to the enhanced plasma temperature and density.[17,24]

Trailing plasma surrounds the dense pinch in small-diameter cylindrical loads. Figure 4 shows a stagnated Z pinch in two shadowgrams at wavelengths of 532 nm (a) and 266 nm (b). Rectangular areas in Fig. 4 show the neck presented in Fig. 1(b). It is seen that the diameter of trailing plasma at 532 nm is significantly larger than the visible size of the pinch at 266 nm. The line in the rectangle in shadowgram (a) shows the size of the current-carrying plasma column. X-ray images (d) of the Z pinch are presented in two x-ray ranges, E > 3 keV in the top row and E > 1.2 keV in the bottom row. A magnified fragment of the x-ray image with bright spots is shown in image (c). Dotted lines show that position of necks in shadowgram (b) coincides with bright areas in x-ray image (c). Enhanced radiation is the evidence

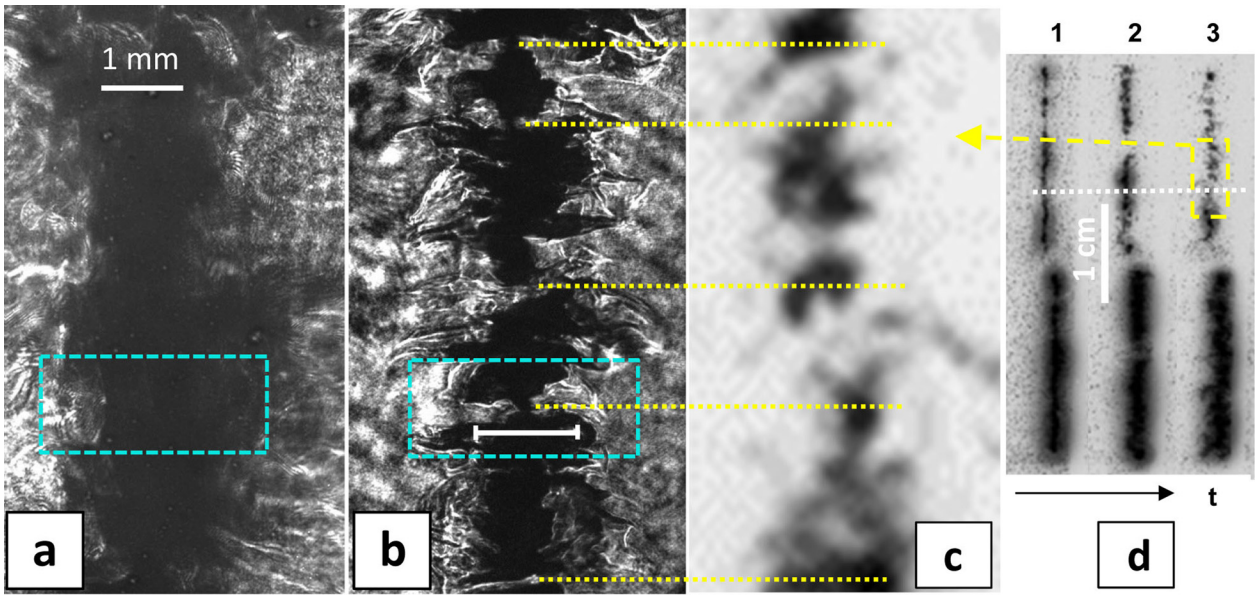

FIG. 4. (a) and (b) Two shadowgrams of the Z pinch in shot 2704 taken at the same time at wavelengths of 532 nm (a) and 266 nm (b). (d) Three x-ray frames of the pinch in two x-ray ranges [see timing in Fig. 1(e)]. A dotted line shows a position of the neck from image (b). A rectangle in frame (3) is magnified in image (c). Dotted lines display spatial position of necks in shadowgram (b) and x-ray image (c).

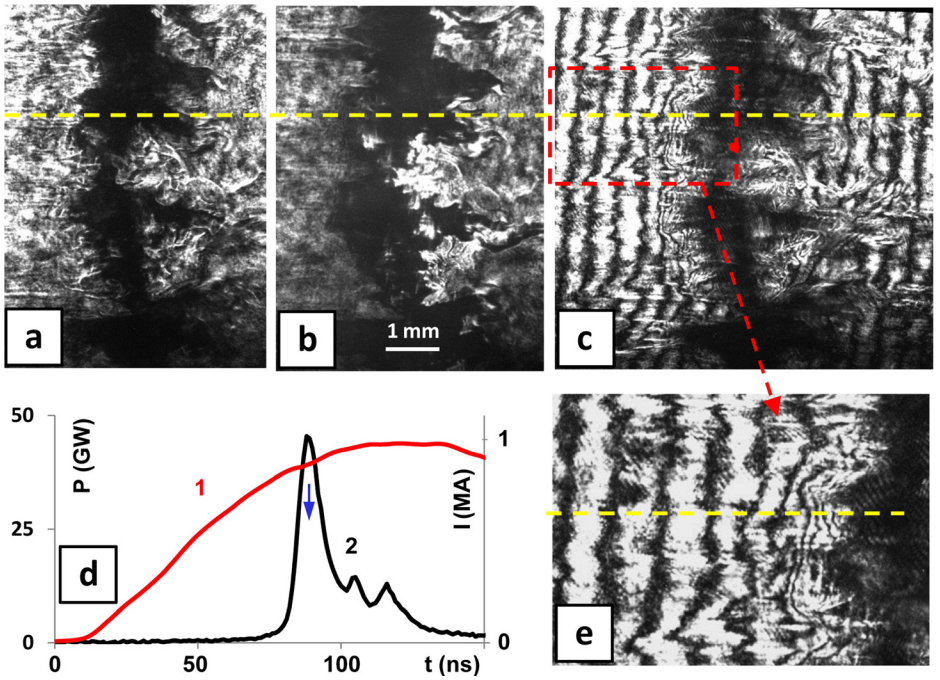

FIG. 5. Laser images of the Z pinch produced by the implosion of the Al star wire-array in shot 2951. Images (a), (b), and (c) represent a shadowgram, Faraday rotation image, interferogram, and magnified fragment of interferogram (e), respectively. The timing diagram (d) shows a current pulse (1), keV x-ray pulse (2), and UV laser frame (arrow). A mismatch angle is 6.7°.

of the higher plasma temperature and enhanced current density in necks.

B. The magnetic field and current near the bulge on the Z pinch

Another configuration of Z-pinch plasma in the star wire array was studied with UV Faraday rotation diagnostics. Implosion in star wire arrays cascade from wire to wire along the rays of the star. Star loads typically produce short-lasting Z pinches without kink instability and with a smaller amount of trailing plasma.[17,25] Images of the Z pinch produced by the implosion of the Al 3-ray star wire array, 2 cm tall, with a mass of 50 μg are shown in Figure 5. Images are taken at the maximum of the x-ray pulse. The total x-ray energy radiated in this shot is 10.2 kJ. The rotation angle and electron density are calculated along the dash line in images (a)–(e) and appropriate reference images. In this direction, the magnetic field is measured near the bulge on the pinch. Interferogram (e) shows a fast decrease of the plasma density in the Z pinch. Lightening and darkening in the Faraday image show magnetic fields with opposite directions.

The rotation angle in Fig. 5 is calculated by the same way as for the shot in Fig. 1. The area with the high plasma gradient is excluded from calculations. The electron plasma density and magnetic field are reconstructed with Abel inversion. Figure 6(a) presents two smoothed fitting lines for the electron plasma density and Faraday rotation angle. Figure 6(b) shows that the reconstructed magnetic field (solid line) fits to the magnetic field calculated for the plasma column 1.2 mm in diameter with total current $I = 0.66$ MA (dashed line). Total current measured at this time by B-dots is 0.89 MA, as seen in Fig. 5(d). The discrepancy can be linked mostly to the experimental error. We also do not exclude that some current can flow out of the radius of plasma of 1.2 mm used for calculation of the current in this shot. A dotted line in Fig. 6(b) shows the magnetic field calculated by formula (2). Deviation of this line from the reconstructed field is 10%–15%. A small enough error allows for estimation of the magnetic field by formula (2) without the reconstruction of the electron density and B-field with Abel inversion.

C. Study of wire-array Z pinches at current of 1.4–1.6 MA

The UV Faraday rotation diagnostic was applied to Z pinches at the enhanced current with a LCM on a pulse-forming-line of the Zebra generator. The current multiplier implemented at NTF provided a maximum current of 1.7 MA in wire-array Z pinches.[19,20] Current in the Z pinch was measured by three calibrated B-dots installed on the top of the return-current cage. Loads were optimized for the LCM regime. Wire arrays with a smaller initial inductance and higher mass compared to the regular 1 MA regime were used. We studied implosions of Al cylindrical arrays with diameters of 12 mm and 16 mm and three- and four-ray star

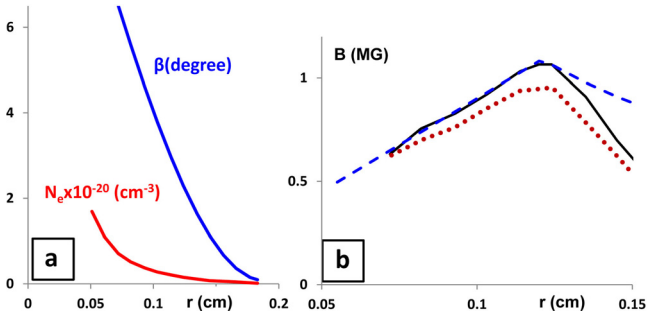

FIG. 6. (a) Fitting lines calculated for the Faraday angle and electron plasma density in shot 2951 along the dashed line in Fig. 5. (b) The reconstructed magnetic field in the pinch (solid line), the magnetic field calculated for current $I = 0.66$ MA in the plasma column 1.21 mm in diameter (dashed line), and B-field estimated by formula (2), dotted line.

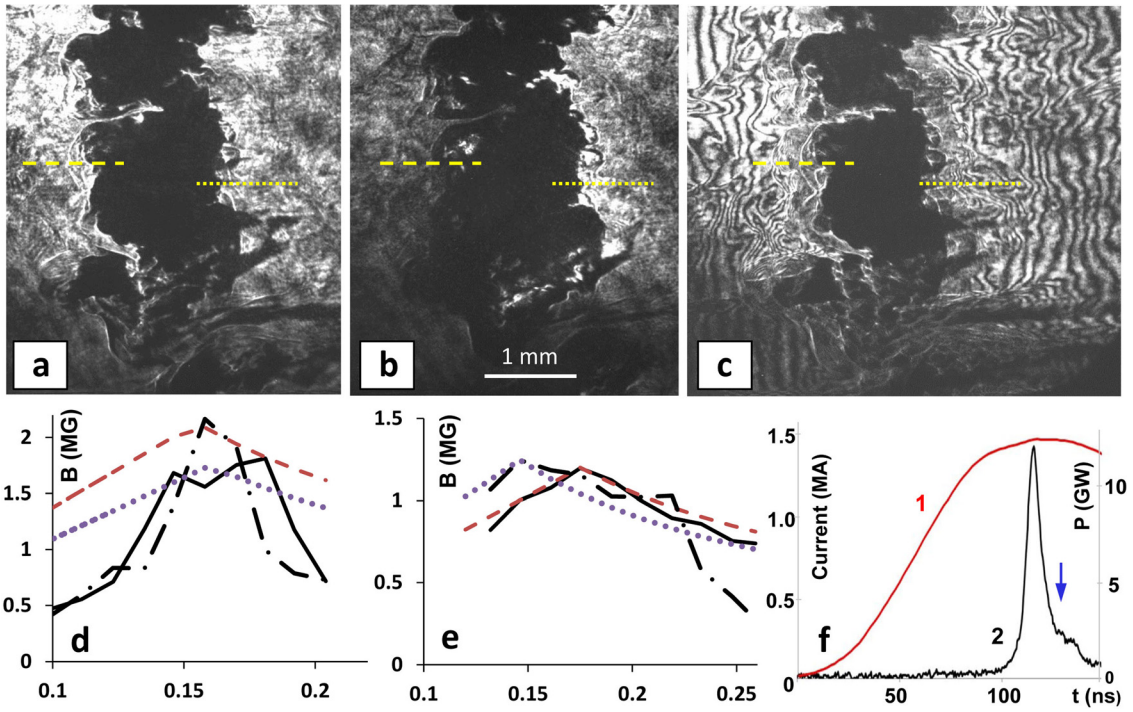

FIG. 7. UV laser images show a central part of the Z pinch produced by implosion of the 3-ray Al star wire array in shot 3675. Images (a)–(c) represent a shadowgram, Faraday image, and interferogram. Dashed and dotted lines show directions of processing. (d) and (e) Reconstructed magnetic fields (solid and dotted-dashed lines) and magnetic fields modelled for a plain current distribution (dashed and dotted lines) for left (d) and right sides (e). (f) The timing diagram with current (1), keV x-ray pulse (2), and UV frames (arrow). A mismatch angle of polarizers is 6.7°.

wire arrays, 1 cm tall, with masses of 70–75 μg. Cylindrical loads imploded to the Z pinch with a large amount of dense non-imploded and trailing mass. This made it difficult to use interferometry for measurement of the plasma density due to the dense trailing plasma near the pinch, tangled structure of fringes, and the absence of the non-distorted fringes on interferograms. Quantitative study of the magnetic field was not possible in this case. Star wire arrays imploded with a smaller amount of trailing mass but Z pinches with enhanced masses were also surrounded by dense plasma at the stagnation stage. Interferometry was able to make quantitative measurements only at the end of stagnation when plasma was mostly collected in the vicinity of the pinch. This allowed a reconstruction of magnetic fields in Z pinch plasma. Current in star loads with LCM was in the range of 1.4–1.5 MA.

Images of the star wire-array Z pinch at current of 1.5 MA are shown in Figure 7. A 3-ray Al load, 1 cm tall, consists of 15 wires 15 μm in diameter placed on diameters of 14/12/10/8/6 mm. The total x-ray energy radiated in this shot is 13.4 kJ. Images (a)–(c) represent a shadowgram, Faraday image, and interferogram, respectively. Dashed and dotted lines in images (a)–(c) show the directions for the processing of the images on the left and right sides. UV images are taken 14 ns after the maximum of the x-ray pulse as shown in the timing diagram (f). Magnetic fields reconstructed on the left and right sides of images are presented in diagrams (d) and (e), respectively.

Processing the Faraday images in shots with LCM is the same as in regular shots but additional issues arise due to larger load masses and higher plasma density. Interpretation of tangled fringes in dense plasma creates additional uncertainty for plasma density measurements and increases the noise in the Faraday image in the area of small plasma density N_e and rotation angle β. Magnetic fields reconstructed at left side (d) and right side (e) of the Z pinch are displayed by two curves that were calculated for two interpretations of plasma density $N_e(r)$ and rotation angle $\beta(r)$ in the range of experimental errors. Dashed and dotted lines show the reconstructed B-fields and solid and dotted-dashed curves present magnetic fields modelled for current in the plasma column with a radius of R_o. The average radius of the current-carrying plasma column is 1.6 mm in both sides of the Z pinch. Calculated average currents are 1 MA and 1.5 MA in the right and left sides of the pinch, respectively. Current calculated from B-dot data is 1.46 MA. The estimated error is ±30%. According to these measurements, current flows in the Z pinch after the main x-ray pulse, and it is distributed in the area of trailing plasma.

Al K-shell time-integrated spectra and pinhole images from this shot were used for characterization of Z-pinch plasma. Spectra were taken at the same time as UV images in Fig. 7. Images showed development of kink instability after the peak of the x-ray pulse. Comparison of the experimental spectrum PrismSpect simulations[29] showed the best fit at the electron plasma temperature of 450 ± 30 eV.

IV. CONCLUSIONS

The magnetic field is investigated in the stagnated Z pinch at current of 0.5–1.5 MA using the Faraday rotation diagnostic at the wavelength of 266 nm. Current in plasma is reconstructed from the magnetic field $B(r)$ using simple

models of current flowing in a homogeneous plasma column. It is found that current flowing in a wide trailing plasma can be higher than current in the dense narrow pinch. Trailing plasma surrounds the stagnated Z pinch in the Zebra generator at current up to 1.6 MA. This trailing plasma is well seen in the vicinity of necks on the pinch at the wavelength of 532 nm. A magnetic field of modelled current with the enhanced density in the neck is in agreement with the experimental curve for the *B*-field. In this current distribution, the main portion of current flows in the large-size trailing plasma and but >10% of current can flow in the narrow neck. The enhanced current in the neck can explain bright radiation spots in x-ray images of the pinch.

Current flows in the trailing plasma heated by radiation of the main x-ray pulse. We suggest that necks in the wire-array Z pinch are not formed during the compression of the plasma column by the sausage instability. Plasma instabilities at the ablation and implosion stages[30] result in the inhomogeneous implosion[31,32] and formation of necks at points of collision of plasma bubbles.[24,26] By this way, necks, trailing plasma, and the current profile in the wire-array Z pinch are created by the inhomogeneous implosion. The complicated structure of the Z pinch is formed under the influence of the further implosion of non-imploded material on the pinch and development of plasma instabilities.

A distribution of current in the large-size trailing plasma can prevent the formation of strong magnetic fields in the stagnated Z pinch. Magnetic fields in the range of 1–2 MG are measured in several series of shots at the Zebra generator with maximum current up to 1.6 MA. Stronger magnetic fields with $B \gg 1$ MG are not found in shots with large mismatch angles $\beta_0 > 7°$. However, we do not exclude strong magnetic field in some plasma phenomena like micro-pinches,[24] which collapse for the short time, and are difficult for observation with laser framing diagnostics.

ACKNOWLEDGMENTS

The authors thank A. M. Covington for supporting this work and V. L. Kantzyrev and A. S. Chuvatin for realization of LCM at the Zebra generator. This work was supported by the DOE Grant No. DE-SC0008824 and DOE/NNSA Grant No. DE-NA 0002075.

[1]C. Deeney, R. Douglas, R. B. Spielman, T. J. Nash, D. L. Peterson, P. L'Eplattenier, G. A. Chandler, J. F. Seaman, and K. W. Struve, Phys. Rev. Lett. **81**, 4883 (1998).
[2]M. E. Cuneo, E. M. Wasiman, S. V. Lebedev, J. P. Chittenden, W. A. Stygar, G. A. Chandler, R. A. Vesey, E. P. Yu, T. J. Nash, D. E. Bliss, G. S. Sarkisov, T. C. Wagoner, G. R. Bennett, D. B. Sinars, J. L. Porter, W. W. Simpson, L. E. Ruggles *et al.*, Phys. Rev. E **71**, 046406 (2005).
[3]C. A. Coverdale, C. Deeney, B. Jones, J. W. Thornhill, K. G. Whitney, A. L. Velikovich, R. W. Clark, Y. K. Chong, J. P. Apruzese, J. Davis, and P. D. LePell, IEEE Trans. Plasma Sci. **35**, 582 (2007).
[4]B. Jones, J. P. Apruzese, A. J. Harvey-Thompson, D. J. Ampleford, C. A. Jennings, S. B. Hansen, N. W. Moore, D. C. Lamppa, D. Johnson, and M. C. Jones, Phys. Plasmas **22**, 020706 (2015).
[5]M. R. Gomez, S. A. Slutz, A. B. Sefkow, D. B. Sinars, K. D. Hahn, S. B. Hansen, E. C. Harding, P. F. Knapp, P. F. Schmit, C. A. Jennings *et al.*, Phys. Rev. Lett. **113**, 155003 (2014).
[6]V. V. Alexandrov, I. N. Frolov, M. V. Fedulov, E. V. Grabovsky, K. N. Mitrofanov, S. L. Nedoseev, G. M. Oleinik, I. Yu. Porofeev, A. A. Samokhin, P. V. Sasorov, V. P. Smirnov, G. S. Volkov, M. M. Zurin, and G. G. Zukakischvili, IEEE Trans. Plasma Sci. **30**, 559 (2002).
[7]S. V. Lebedev, R. Aliaga-Rossel, S. N. Bland, J. P. Chittenden, A. E. Dangor, M. G. Haines, and M. Zakaullah, Phys. Rev. Lett. **84**, 1708 (2000).
[8]F. S. Felber, F. J. Wessel, N. C. Wild, H. U. Rahman, A. Fisher, C. M. Fowler, M. A. Liberman, and A. L. Velikovich, J. Appl. Phys. **64**, 3831 (1988).
[9]E. Kroupp, G. Rosenzweig, A. Fisher, Y. Maron, J. Giuliani, W. Thornhill, A. Velikovich, and A. Dasgupta, Bull. Am. Phys. Soc. **59**, 181 (2014).
[10]D. Mariscal, C. McGuffey, J. Valenzuela, M. Wei, J. Chittenden, N. Niasse, R. Presura, S. Haque, M. Wallace, A. Arias, A. Covington, H. Sawada, P. Wiewior, and F. Beg, Appl. Phys. Lett. **105**, 224103 (2014).
[11]V. V. Ivanov, G. S. Sarkisov, P. Laca, V. I. Sotnikov, V. L. Kantsyrev, B. Jones, C. A. Coverdale, P. D. LePell, C. Deeney, K. W. Struve, A. L. Astanovitskiy, D. Fedin, B. Le Galloudec, V. Nalajala, I. Shrestha, and T. E. Cowan, IEEE Trans. Plasma Sci. **34**, 2247 (2006).
[12]G. S. Sarkisov, A. S. Shikanov, B. Etlitcher, S. Attelan, and C. Rouile, JETP Lett. **61**, 485 (1995).
[13]M. Tatarakis, R. Aliaga-Rossel, A. E. Dangor, and M. G. Haines, Phys. Plasmas. **5**, 682 (1998).
[14]A. Yu. Labetsky, R. B. Baksht, V. I. Oreshkin, A. G. Rousskikh, and A. V. Shishlov, IEEE Trans. Plasma Sci. **30**, 524 (2002).
[15]N. Qi, R. R. Prasad, K. Campbell, P. Coleman, M. Krishnan, B. V. Weber, S. J. Stephanakis, and D. Mosher, IEEE Trans. Plasma Sci. **26**, 1127 (1998).
[16]V. V. Ivanov, J. P. Chittenden, S. D. Altemara, N. Niasse, P. Hakel, R. C. Mancini, D. Papp, and A. A. Anderson, Phys. Rev. Lett. **107**, 165002 (2011).
[17]V. V. Ivanov, J. P. Chittenden, R. C. Mancini, D. Papp, N. Niasse, S. D. Altemara, and A. A. Anderson, Phys. Rev. E **86**, 046403 (2012).
[18]V. V. Ivanov, A. A. Anderson, D. Papp, A. L. Astanovitskiy, B. R. Talbot, J. P. Chittenden, and N. Niasse, Phys. Rev. E **88**, 013108 (2013).
[19]A. Chuvatin, V. L. Kantsyrev, L. I. Rudakov, M. E. Cuneo, A. L. Astanovitskiy, R. Presura, A. S. Safronova, W. Cline, K. M. Williamson, I. Shrestha *et al.*, Phys. Rev. Spec. Top.–Accel. Beams **13**, 010401 (2010).
[20]V. L. Kantsyrev, A. S. Chuvatin, A. A. Esaulov, A. S. Safronova, L. I. Rudakov, A. Velikovich, K. M. Williamson, G. C. Osborne, I. K. Shrestha, M. E. Weller, and V. V. Shlyaptseva, Phys. Plasmas. **20**, 070702 (2013).
[21]G. S. Sarkisov, Instrum. Exp. Tech. **39**, 727 (1996).
[22]V. V. Ivanov, A. A. Anderson, D. Papp, B. R. Talbot, J. P. Chittenden, N. Niasse, and I. A. Begishev, IEEE Trans. Plasma Sci. **42**, 1153 (2014).
[23]S. A. Altemara, D. Papp, V. V. Ivanov, A. A. Anderson, A. L. Astanovitskiy, and V. Nalajala, IEEE Trans. Plasma Sci. **40**, 3378 (2012).
[24]V. V. Ivanov, D. Papp, A. A. Anderson, B. R. Talbot, A. L. Astanovitskiy, V. Nalajala, O. Dmitriev, J. P. Chittenden, N. Niasse, S. A. Pikuz, and T. A. Shelkovenko, Phys. Plasmas. **20**, 112703 (2013).
[25]V. V. Ivanov, V. I. Sotnikov, A. Haboub, A. P. Shevelko, A. L. Astanovitskiy, A. Morozov, E. D. Kazakov, and S. D. Altemara, Phys. Rev. Lett. **100**, 025004 (2008).
[26]V. V. Ivanov, V. I. Sotnikov, J. M. Kindel, P. Hakel, R. C. Mancini, A. L. Astanovitskiy, A. Haboub, S. D. Altemara, A. P. Shevelko, E. D. Kazakov, and P. V. Sasorov, Phys. Rev. E **79**, 056404 (2009).
[27]G. S. Sarkisov, Quantum Electron. **26**, 799 (1996).
[28]B. Jones, C. Deeney, J. L. McKenney, C. J. Garasi, T. A. Mehlhorn, A. C. Robinson, S. E. Wunsch, S. N. Bland, S. V. Lebedev, J. P. Chittenden *et al.*, Phys. Rev. Lett. **95**, 225001 (2005).
[29]J. J. MacFarlane, I. E. Golovkin, P. Wang, P. R. Woodruff, and N. A. Pereira, High Energy Density Phys. **3**, 181 (2007).
[30]S. V. Lebedev, F. N. Beg, S. N. Bland, J. P. Chittenden, A. E. Dangor, M. G. Haines, K. H. Kwek, S. A. Pikuz, and T. A. Shelkovenko, Phys. Plasmas. **8**, 3734 (2001).
[31]D. B. Sinars, M. E. Cuneo, E. P. Yu, D. E. Bliss, T. J. Nash, J. L. Porter, C. Deeney, M. G. Mazarakis, G. S. Sarkisov, and D. F. Wenger, Phys. Rev. Lett. **93**, 145002 (2004).
[32]V. V. Ivanov, V. I. Sotnikov, G. S. Sarkisov, T. E. Cowan, S. N. Bland, B. Jones, C. A. Coverdale, C. Deeney, P. J. Laca, A. L. Astanovitskiy, and A. Haboub, Phys. Rev. Lett. **97**, 125001 (2006).